BMC Medical Imaging

RESEARCH Open Access

Monoexponential, biexponential, stretched exponential and diffusion kurtosis models of diffusion-weighted imaging: a quantitative differentiation of solitary pulmonary lesion

Ke Wang[1*] and Guangyao Wu[2]

Abstract

Background Diffusion-weighted imaging (DWI) can be used for quantitative tumor assessment. DWI with different models may show different aspects of tissue characteristics.

Objective To investigate the diagnostic performance of parameters derived from monoexponential, biexponential, stretched exponential magnetic resonance diffusion weighted imaging (DWI) and diffusion kurtosis imaging (DKI) in differentiating benign from malignant solitary pulmonary lesions (SPLs).

Method Forty-four SPL subjects were selected according to the inclusion criteria. All patients underwent conventional and multi-b DWI sequences. Monoexponential DWI and DKI model were fitted using least square method. Levenberg-Marquardt nonlinear fitting biexponential and stretched exponential DWI. Region of interests (ROIs) were described manually. Parameters between benign and malignant SPLs were compared using independent sample t test or the Mann-Whitney U test. Receiver operating characteristic (ROC) curves analysis was used to investigate the diagnostic performance of different DWI parameters. Correlation between all parameters were evaluated by using Spearman correlation.

Result ADC, ADC_{slow}, α, DDC and D_{app} values were significantly lower in malignant SPL than in benign SPL ($P < 0.001$). K_{app} was significantly higher in malignant SPL than in benign SPL ($P < 0.001$). Among all subjects, ADC_{slow} was significantly lower than ADC ($P < 0.05$), while DDC and D_{app} were significantly higher than ADC ($P < 0.05$). When observing the ROC curves for distinguishing benign and malignant SPL, the AUC values of ADC, ADC_{slow}, DDC, D_{app}, and K_{app} were 0.904, 0.815, 0.942, 0.93, and 0.815, respectively. The DDC value has the highest area under ROC curve value. DeLong analysis showed no statistically significant difference in the area under ADC, DDC, and D_{app} curves. There were strong correlations among ADC, ADC_{slow}, ADC_{fast}, f, α, DDC, D_{app}, and K_{app} ($P < 0.001$).

Conclusion Multi-b DWI is a promising method for differentiating benign from malignant SPLs with high diagnostic accuracy. In addition, the DDC derived from stretched-exponential model is the most promising DWI parameter for the differentiation of benign and malignant SPLs.

*Correspondence:
Ke Wang
wangke2013@whu.edu.cn

Full list of author information is available at the end of the article

Trail registration This study was a clinical trail study, with study protocol published at ClinicalTrails. Retrospectively registered number ChiCTR2300074258, date of registration 02/08/2023.

Keywords Solitary pulmonary lesion, Diffusion weighted imaging, Intravoxel incoherent motion, Stretched exponential, Diffusion kurtosis imaging

Background

Lung cancer presently stands as the second morbidity tumor both in males and females, as well as the key culprit for cancer-related fatality worldwide [1]. The most common manifestation of lung cancer is a solitary pulmonary lesion (SPL), which contain both nodule and mass. The nature of SPL is indefinite, with some being malignant tumors and many presenting as benign lesions, including tuberculomas, inflammatory pseudo-tumors, and hamartomas, among others. Hence, it is imperative to determine the properties of SPLs before treatment.

Computed tomography (CT) is the most common diagnostic method for SPL. However, CT encounters difficulties in accurately determining the benign or malignant nature of some SPLs. Although the evaluation of tumor vascular distribution through contrast-enhanced CT has been shown to be useful in distinguishing malignant nodules from benign ones, some active granulomas or highly vascular benign tumors may also produce false positive results [2, 3]. ^{18}F-fluorodeoxyglucose (^{18}F-FDG) positron emission tomography (PET) is a non-invasive method that can detect SPL with high sensitivity but low specificity, with 90.1% and 39.8%, respectively [4]. However, there are also reports that ^{18}F-FDG PET can produce false positive and false negative results in distinguishing well-differentiated lung adenocarcinoma and inflammatory lesions [5–8].

Diffusion-weighted imaging (DWI) can be used for quantitative tumor assessment. Water diffusion is restricted in malignant tumor tissues due to an increase in cell number, larger cell nuclei accompanied by more abundant macromolecules, a larger nucleus/cytoplasm ratio, and less extracellular space relative to normal tissue. This forms the basis for tumor quantification [9]. However, some studies have reported limitations in using ADC to differentiate SPLs. ADC values calculated using a single-index model may not accurately reflect the diffusion of water molecules in vivo because it is affected by microcirculation in capillaries [10]. Moreover, contrary to the Gaussian diffusion assumption of conventional diffusion imaging, there are "barriers" in many biological tissues, such as cell membranes and compartments, which can change the probability density function (PDF) of water diffusion. This causes water diffusion to be not an exact Gaussian distribution, but in reality, a non-Gaussian distribution [11].

Previous researchers had proposed that the bi-exponential (also known as intravoxel incoherent motion, IVIM) or stretched exponential DWI models and diffusion kurtosis imaging (DKI) may provide more accurate water diffusion information [12–14]. The bi-exponential intravoxel incoherent motion DWI model proposed by Le Bihan et al. [12] may allow separation of water diffusion from microcirculation. However, its value has not been well evaluated until recent years. The stretched exponential DWI model proposed by Bennett et al. [13] was used to describe the heterogeneity of diffusion rate and distributed diffusion effect in vivo. DKI had been used to measure non-Gaussian diffusion and may better characterize normal and pathological tissues than diffusion tensor imaging [14]. Exploring and comparing their roles in distinguishing between benign and malignant SPLs would be valuable because DWI with different models may show different aspects of tissue characteristics. However, to our knowledge, there had been no studies comparing these different diffusion imaging methods in identifying benign and malignant SPLs. Therefore, the aim of this study was to quantitatively compare the potential of various derived diffusion parameters from multi-b values and different signal attenuation fitting in distinguishing between benign and malignant SPLs.

Methods

Patients

This prospective study was approved by the Institutional Review Board of Renmin hospital of Wuhan university (RMKYC2016-281) on September 1, 2016, and written informed consent was obtained from all participants. From October 2016 to June 2019, a total of 57 SPL patients participated in this study. The inclusion criteria were as follows: (a) the lesion had a short diameter greater than or equal to 1 cm on CT scan; (b) no history of anti-inflammatory or radiotherapy prior to examination and no acute inflammation; (c) no contraindications for MRI examination; (d) the pathological diagnosis was confirmed by CT-guided lung needle puncture biopsy or surgical diagnosis within 10 days after MRI. Thirteen patients were excluded from the study for one or more of the following reasons: (a) uncertain pathological results ($n=5$); (b) imaging quality or artifacts caused by motion during examination were unsatisfactory ($n=3$); (c) the short axis diameter of the nodules was less than 1 cm, and there was not enough solid area to place regions of interest (ROIs) of interest ($n=5$). Finally, 44 patients met all criteria and were included in this study.

MRI protocol

All patients underwent imaging using a 3-T MR imaging device (Siemens trio 3.0; Siemens Medical Systems, Germany) and an 8-channel body coil (Siemens Medical Systems). Patients were positioned in a supine position and instructed to breathe calmly and evenly during the routine MR imaging using a fast spin-echo sequence. Axial T1-weighted images were acquired using a volumetric interpolated breath-hold examination (VIBE) sequence with a repetition time (TR)/echo time (TE) of 3.25ms/1.01ms, a slice thickness of 5 mm, a field of view (FOV) of 240 mm×320 mm, and a matrix of 192×192. Axial T2-weighted images with fat suppression were obtained using TR/TE of 2500ms/73ms, a slice thickness of 5 mm, a FOV of 240 mm×320 mm, and a matrix of 192×192. Coronal T2-weighted images were obtained using TR/TE of 1000ms/86ms, a slice thickness of 5 mm, a FOV of 340 mm×340 mm, and a matrix of 192×192. For the multi-b-value DWI sequence, DWI was acquired using a single-shot echo-planar imaging (SS-EPI) sequence in the axial plane with TR/TE of 4600ms/83ms, a slice thickness of 5 mm, no gap, a FOV of 320 mm x 320 mm, and a matrix of 128×128. The b-value was set from 0 to 2000 s/mm^2 (0, 50, 100, 150, 200, 250, 300, 500, 700, 900, 1000, 1500, and 2000 s/mm^2), with an average excitation of b=0–800 s/mm^2 once, b=900–1000 s/mm^2 twice, b=1500 s/mm^2 three times, and b=2000 s/mm^2 four times. Diffusion was performed in three orthogonal directions for single-exponential, bi-exponential, stretched-exponential models, and DKI fitting. Considering the scanning time, patients maintained free breathing in small degree without breath-holding or respiratory triggering during the multi-b DWI scanning process. The total acquisition time for DWI was 6 min and 37 s. Based on previous studies, the selection of b-value distribution and signal number in our study is a trade-off between acquisition time and signal-to-noise ratio in the model.

Data analysis and processing

The acquired multi-b-value DWI images were transferred to our internal processing software (MATLAB 2013b) for analysis. They were independently processed by two thoracic radiologists with 5 and 20 years of chest MR imaging experience, respectively, who were blinded to the histopathological results. Firstly, non-rigid registration software was used for image registration. Then, the registered images were used for fitting multiple mathematical models.

Considering the use of all b-values for data fitting might better reflect the actual state of water molecule diffusion, a single exponential model was used to compute ADC values from all 13 fitted b-values: where S_b represents signal intensity in the presence of diffusion-sensitive gradients and S_0 represents signal intensity in the absence of diffusion. The fitting formula was as follows:

$$S_b/S_0 = exp\,(-b \times\ ADC) \tag{1}$$

Three parameters, namely perfusion fraction (f), pseudo ADC (ADC_{fast}), and true ADC (ADC_{slow}), were analyzed using a bi-exponential model for incoherent motion within the voxel. The b-values selected for this analysis were 0, 50, 100, 150, 200, 250, 300, 500, 700, 900, and 1000 s/mm^2. The formula is as follows:

$$\frac{S_b}{S_0} = [f \times\ exp\,(-b \times\ ADC_{fast})] + [(1-f) \times\ exp\,(-b \times\ ADC_{slow})] \tag{2}$$

In the stretched exponential DWI model, α represents the heterogeneity index of water molecule diffusion. The data was fitted using b-values of 200, 500, 1000, 1500, and 2000 s/mm^2, with b-values below 200 s/mm^2 excluded to avoid perfusion effects. The heterogeneity index (α) and distributed diffusion coefficient (DDC) were calculated using the following formula:

$$S_b/S_0 = exp\,[-\,(b \times\ DDC)^{\alpha}\,] \tag{3}$$

Where α was associated with the heterogeneity of water molecule diffusion within the body and varies between 0 and 1. Higher α value indicated lower voxel diffusion heterogeneity, approaching single exponential decay. DDC represented the average diffusion rate within the body.

The diffusion kurtosis model is described as follows: where D_{app} is the ADC corrected by non-Gaussian model and K_{app} is the apparent diffusion kurtosis, which measures the degree of non-Gaussian displacement. For DKI, data was fitted using b-values of 200, 500, 1000, 1500, and 2000 s/mm^2, with b-values below 200 s/mm^2 excluded to avoid perfusion effects. The fitting is done using the following formula:

$$S_b/S_0 = exp\,(-b \times\ D_{app} + 1/6b^2 \times\ D_{app}^2 \times\ K_{app}) \tag{4}$$

The fitting methods utilized in previous studies typically involved linear regression for the monoexponential and diffusion kurtosis models, and the Levenberg-Marquardt algorithm for the biexponential and stretched exponential models using the least squares fitting technique.

Two chest radiologists (W.K and W.GY) independently analyzed all images without knowledge of patients' pathology or clinical information. For each patient, each radiologist placed a region of interest (ROI) within the solid tumor component on the b_{1000} image to obtain measurement results. The ROI size ranged from 20 to 45 mm^2 (mean area, 37 mm^2) and avoided areas of necrosis, cysts, hemorrhage, large vessels, edema, and calcifications to ensure more accurate measurements. Then, the

selected ROI on the b_{1000} image was copied onto all other parameter maps from the same patient.

Statistical analysis

The statistical analysis was performed using SPSS software (version 23.0; SPSS, Chicago, Ill). The average results of each parameter from two radiologists were used for quantitative statistical analysis. The Mann-Whitney U test was used to compare each parameter between benign and malignant SPL. The Wilcoxon signed-rank test was used to compare the ADC and ADC_{slow} values calculated from all subjects. Spearman rank correlation was used to evaluate the correlation between all parameters, and Pearson correlation was used to characterize the correlation between each parameter. Receiver operating characteristic (ROC) curves were used to evaluate the area under the ROC curve (AUC) and determine which parameter was best for distinguishing between benign and malignant SPL, and the DeLong analysis was used to evaluate the differences between parameters. The cut-off point was chosen by maximizing the Youden index. The sensitivity and specificity of each diffusion parameter threshold were then determined for differentiating between benign and malignant SPL. The intraclass correlation coefficient (ICC) was used to evaluate the inter-observer reliability between two independent quantitative analyses. Results with a *p*-value less than 0.05 were considered significant.

Results

General clinical data

44 subjects including 34 males and 10 females, with an age range of 25–68 years and a mean age of 46 years. Twenty-eight patients had a smoking history of more than 10 pack-years (the average number of packs smoked per day multiplied by the number of years smoked). Among the 44 patients, 10 patients only underwent biopsy, 22 cases underwent both biopsy and surgical treatment, and 12 patients underwent surgery without a prior biopsy. 30 (68%) patients were diagnosed with malignant SPL based on pathological examination, and the remaining 14 (32%) were diagnosed with benign SPL. Among the 30 malignant lesions, there were 12 cases of squamous cell carcinoma, 15 cases of adenocarcinoma, 1 case of adenosquamous carcinoma, and 2 cases of small cell lung cancer. Among the 14 benign lesions, there were 4 cases of tuberculoma, 3 cases of inflammatory pseudotumor, 3 cases of granulomatous inflammation, 3 cases of hamartoma, and 1 case of sclerosing hemangioma. The lesion sizes for the benign and malignant groups were 4.56 cm (1.27–17.82) and 4.8 cm (1.32–10.26), respectively, with no significant difference between the two groups ($P>0.05$).

Quantitative comparison of diffusion parameters between benign and malignant SPLs

The intraclass correlation coefficient (ICC) between the two diagnosing physicians for all DWI and DKI parameters was greater than 0.75, indicating excellent reproducibility of quantitative parameter evaluation between observers. Our results were analyzed based on the average results of the two physicians. Figures 1 and 2 showed representative T1 and T2 images, as well as ADC, ADC_{fast}, ADC_{slow}, f, α, DDC, D_{app}, and K_{app} maps for benign and malignant SPL, respectively. Table 1 showed the quantitative comparison of diffusion parameters between benign and malignant SPL groups. The ADC, ADC_{slow}, α, DDC, and D_{app} values were significantly lower in malignant SPL than in benign SPL ($p<0.001$), while K_{app} was significantly higher in malignant SPL than in benign SPL ($p<0.001$). No differences were found between the two groups for the perfusion-related parameters ADC_{fast} and f. Among all subjects, ADC_{slow} was significantly lower than ADC ($p<0.001$), while DDC and D_{app} were significantly higher than ADC ($p<0.001$) (Fig. 3).

Receiver operating characteristic curve to differentiate benign and malignant SPLs

When observing the receiver operating characteristic curve to differentiate between benign and malignant solitary pulmonary lesions (SPL) (Fig. 4), the area under the curve (AUC) values of ADC, ADC_{slow}, DDC, D_{app}, and K_{app} were 0.904, 0.815, 0.942, 0.93, and 0.815, respectively. DDC demonstrated the largest area under the curve. Table 2 demonstrated the sensitivity and specificity of diffusion parameters at the optimal cut-off values for distinguishing between benign and malignant SPL. DeLong's analysis revealed no statistical differences in the AUC between ADC, DDC, and D_{app} curves.

Correlation analysis between ADC and diffusion parameters

The quantitative correlation analysis revealed a strong correlation ($p<0.001$) between ADC and the diffusion parameters ADC_{slow}, ADC_{fast}, f, α, DDC, D_{app}, and K_{app} (Table 3). All the parameters that reflect tissue diffusion showed significant correlation with each other, while the parameters that reflect tissue perfusion, ADC_{fast} and f, were correlated with diffusion parameters. There was no statistically significant correlation between the parameters that reflect tissue heterogeneity, α and K_{app}. There was a moderate positive correlation between α and ADC values, and a moderate negative correlation between K_{app} and ADC values.

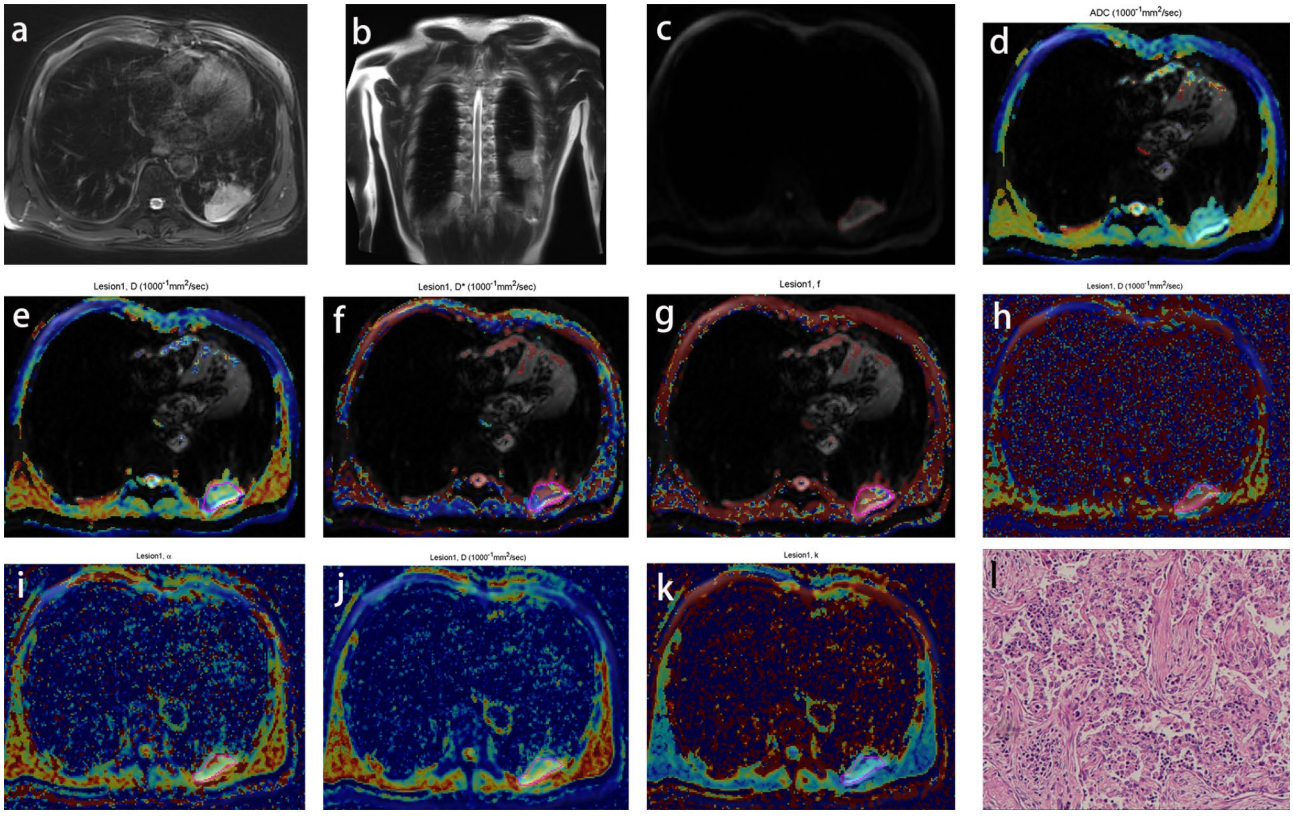

Fig. 1 A case of pneumocytic pseudotumor in the left lung. **a**: Axial T2-weighted fat suppression sequence; **b**: Coronal T2-weighted sequence; **c**: b1000 map with ROI; **d**: ADC map; **e**: D_{slow} map; **f**: D_{fast} map; **g**: f map; **h**: DDC map; **i**: α map; **j**: D_{app} map; **k**: K_{app} map; **l**: HE-stained pathological image (×200) indicates pneumocytic pseudotumor

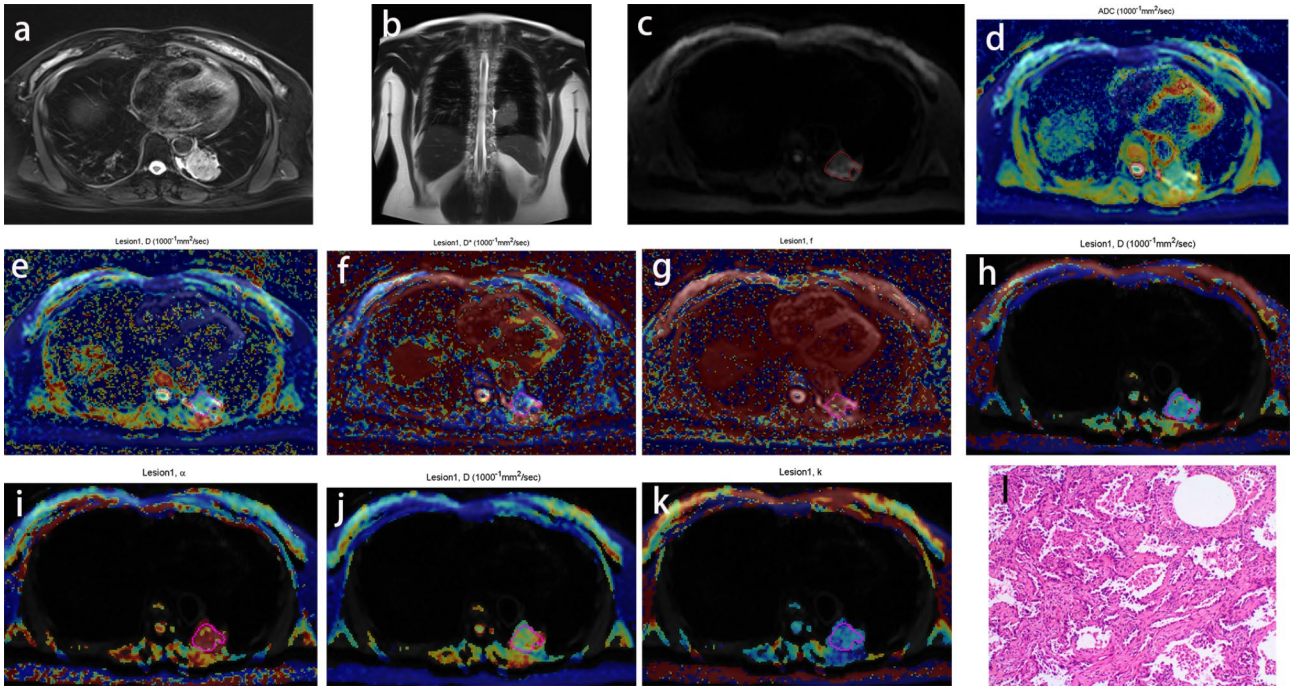

Fig. 2 A case of adenocarcinoma in the left lung. **a**: Axial T2-weighted fat suppression sequence; **b**: Coronal T2-weighted sequence; **c**: b1000 map with ROI; **d**: ADC map; **e**: D_{slow} map; **f**: D_{fast} map; **g**: f map; **h**: DDC map; **i**: α map; **j**: D_{app} map; **k**: K_{app} map; **l**: HE-stained pathological image (×200) indicates invasive adenocarcinoma

Table 1 Comparison of multi-b DWI parameters between benign and malignant SPLs

parameters	benign	malignant	T value	*p* value
ADC ($\times10^{-3}$ mm^2/s)	1.34 ± 0.1	1.18 ± 0.14	6.24	<0.001
ADC_{slow} ($\times10^{-3}$ mm^2/s)	1.17 ± 0.09	1.05 ± 0.08	4.09	<0.001
ADC_{fast} ($\times10^{-3}$ mm^2/s)	12.75 ± 5.07	15.31 ± 6.29	-1.34	0.189
f (%)	25.66 ± 9.3	23.25 ± 8.57	0.85	0.402
α	0.75 ± 0.07	0.63 ± 0.06	5.81	<0.001
DDC ($\times10^{-3}$ mm^2/s)	1.75 ± 0.1	1.56 ± 0.08	7.14	<0.001
D_{app} ($\times10^{-3}$ mm^2/s)	1.59 ± 0.07	1.41 ± 0.08	6.53	<0.001
K_{app}	0.54 ± 0.07	0.64 ± 0.09	-3.74	<0.001

Discussion

In this study, our results showed that the diagnostic performance of DDC and D_{app} was slightly higher than that of the conventional diffusion parameter ADC in distinguishing between malignant and benign SPL. DDC value can be used as the optimal diffusion parameter for discriminating between benign and malignant SPL.

DWI could non-invasively reflect the characteristics of biological tissues by measuring the diffusion properties of water molecules and quantitatively analyzing ADC values. We found that the ADC value of malignant SPL was significantly lower than that of benign SPL. One possible reason for this is that malignant tissue has a higher ratio of cell nucleus, nucleolus, and cytoplasm, with obvious cellular atypia, high cell density, small extracellular space, and irregularities in cell nucleus and cell membrane. These factors may result in more restricted diffusion of water molecules in both extracellular and intracellular spaces, whereas benign SPL has lower cell density and larger extracellular space, resulting in larger ADC values. Study had shown that the diffusion of water molecules in tumors is mainly affected by tumor cell density and the movement of water molecules in the stroma [15]. The cell density of malignant SPL is higher than that of benign SPL, with an increased number of cells per unit volume and a relatively reduced extracellular space, resulting in more restricted diffusion of water molecules and lower ADC values. Therefore, ADC values are a useful method for assessing histological characteristics. Some studies have shown that changes in ADC values occur earlier than morphological changes and can be used to evaluate and detect the effectiveness of tumor treatment [16, 17].

In the IVIM model, we found that the ADC_{slow} value of malignant SPL was significantly lower than that of benign lesions, which was consistent with previous research results. Previous studies had shown that the ADC_{slow} value of lung cancer was significantly lower than that of obstructive atelectasis. Yuan et al. found that malignant SPL has a lower ADC_{slow} value compared to benign SPL [18]. The diffusion coefficient level largely depended on the ratio of intracellular and extracellular space in the tumor. Previous in vivo and in vitro studies had shown

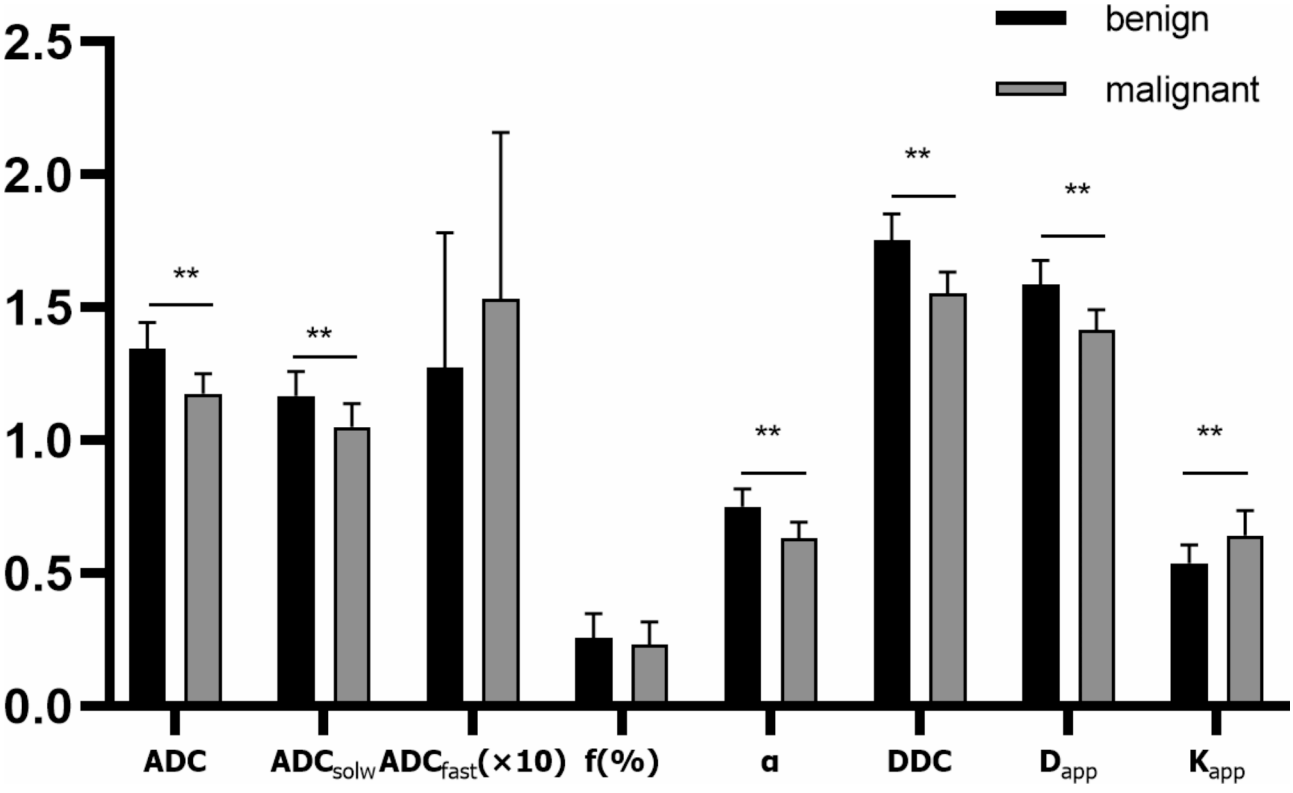

Fig. 3 Bar chart of parameters for benign and malignant groups, ** indicates $P < 0.001$, while the absence of an asterisk indicates no statistical significance

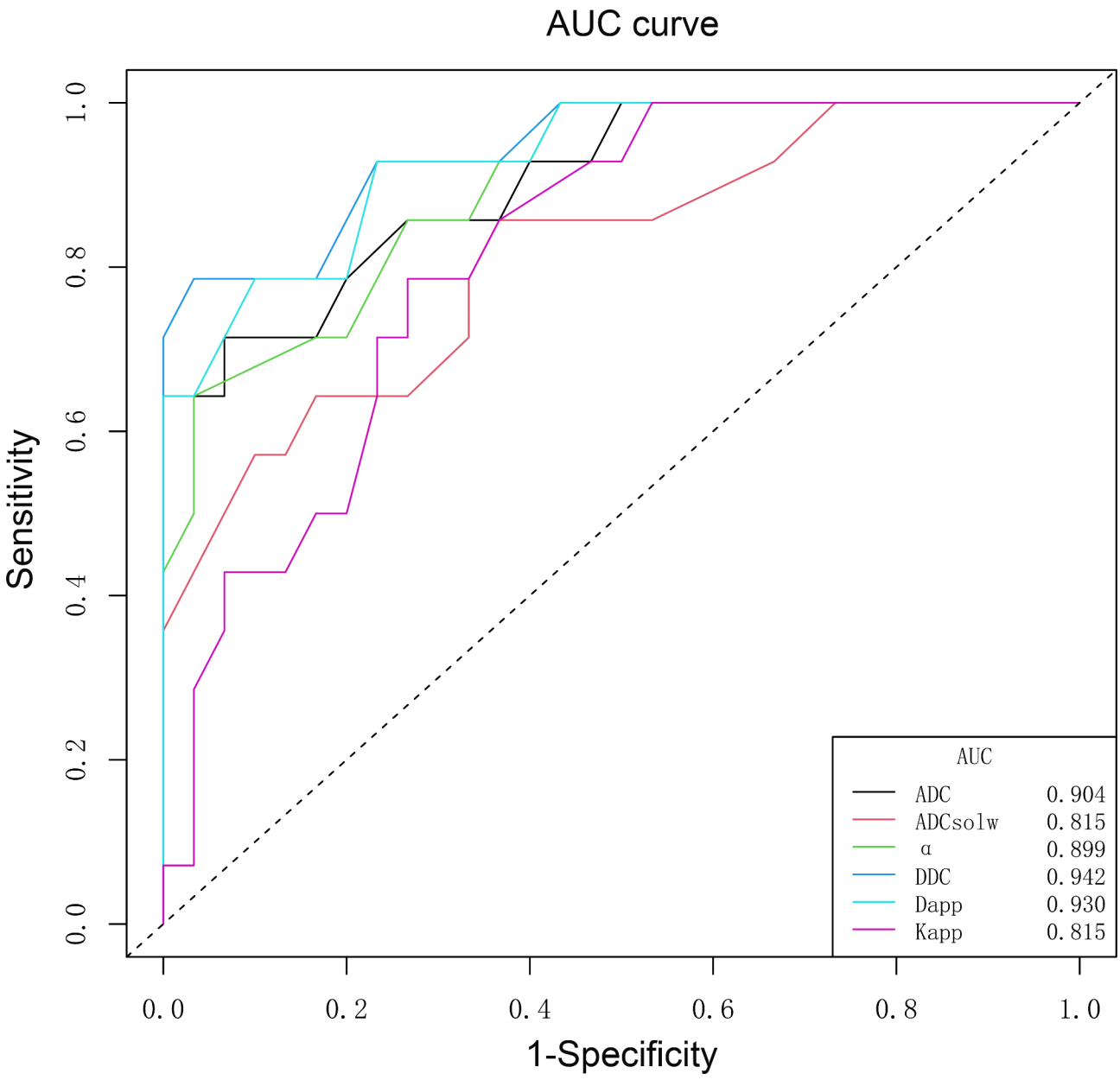

Fig. 4 ROC curves differentiate between benign and malignant SPLs, the AUC values of ADC, ADC_{slow}, DDC, α, D_{app}, and K_{app} were 0.904, 0.815, 0.942, 0.899, 0.93, and 0.815, respectively

Table 2 ROC curve analysis of diagnostic multi-b DWI parameters for benign and malignant SPLs

parameters	AUC	Cut-off	Sensitivity (%)	Specific (%)
ADC($\times 10^{-3}$ mm^2/s)	0.904	1.27	93.33	71.43
ADC_{slow}($\times 10^{-3}$ mm^2/s)	0.815	1.06	63.33	85.71
α	0.899	0.72	96.67	64.29
DDC($\times 10^{-3}$ mm^2/s)	0.942	1.67	96.67	78.57
D_{app}($\times 10^{-3}$ mm^2/s)	0.93	1.47	76.67	92.86
K_{app}	0.815	0.58	73.33	78.57

that the ADC value is closely related to the tumor cell structure [19–21]. This could also be inferred from our research results. Compared with benign lesions, lung cancer cells proliferate faster, showing lower ADC values and ADC_{slow} values. However, the ADC_{fast} and f values did not reflect the difference between benign and malignant SPL, which may be related to the instability of ADC_{fast} and f parameters. Many factors may cause changes in IVIM parameters, such as tumor heterogeneity, technical instability, and fitting errors. Previous studies had shown that low b-value signals are more prone to measurement errors and highly sensitive to signal and

Table 3 Correlation analysis between different parameters derived from different DWI models

parameter	ADC	ADC_{slow}	ADC_{fast}	f	α	DDC	D_{app}
ADC	…	…	…	…	…	…	…
ADC_{slow}	0.933**	…	…	…	…	…	…
ADC_{fast}	-0.599**	-0.652**	…	…	…	…	…
f	0.546**	0.65**	-0.925**	…	…	…	…
α	0.621**	0.546**	-0.227	0.163	…	…	…
DDC	0.97**	0.899**	-0.547**	0.493**	0.704**	…	…
D_{app}	0.945**	0.874**	-0.514**	0.465**	0.666**	0.905**	…
K_{app}	-0.57**	-0.526**	0.176	-0.178	-0.518**	-0.628**	-0.637**

Note: ** indicates $P<0.001$, while the absence of an asterisk indicates no statistical significance

noise changes, which is a challenge to obtaining a good bi-exponential model fit [22, 23]. In addition, although low b-value images were sensitive to vascular perfusion, other volumetric flow phenomena, such as tubular flow or glandular secretion, may cause signal attenuation and are difficult to distinguish from perfusion [24]. Moreover, the pseudo-diffusion coefficient ADC_{fast} reflects the perfusion signal in the microvascular system, and f is the perfusion fraction characterizing the vascular volume fraction. Therefore, the variation of ADC_{fast} and f values may be related to the heterogeneous vascular distribution in the ROI. However, in our study, the drawn ROIs were relatively small, only including a part of the lesion, and for some special benign SPL, such as sclerosing hemangioma, their own vascular components are relatively high, so the ADC_{fast} and f values of benign SPL are more variable, leading to no statistical significance in the difference in ADC_{fast} and f values between benign and malignant SPL. Further researches are needed to use histogram analysis based on the whole volume to distinguish tumor invasiveness and tumor type, and to further evaluate the correlation between ADC_{fast} and f values and tumor heterogeneity, which may yield more convincing results.

The stretching index model overcome the limitations of the fast and slow diffusion compartmental models and their slow exchange in the bi-exponential model. DDC can be considered as a synthesis of various ADCs, indicating the weighted volume fraction of water molecules in the continuous distribution of ADCs within a voxel [13]. α is believed to reflect tissue heterogeneity, and a previous study [25] had shown that the heterogeneity index of malignant tumors is significantly different from that of benign tissues. Our current research indicated that DDC and α were both significantly lower in malignant tumors than in benign lesions, which is similar to previous research results [26]. One possible explanation is that malignant tumor tissue exhibits more diffusion heterogeneity in vivo than benign tissue because it has more histological heterogeneity, such as cellular structural heterogeneity and tortuous angiogenesis. Similar to ADC, DDC is lower in malignant SPL due to high cell density and limited extracellular space, which restricts water molecule diffusion.

As an extension of diffusion tensor imaging (DTI), diffusion kurtosis imaging (DKI) can provide additional measurement parameter K_{app} to characterize the complexity of the microenvironment by measuring the non-Gaussian diffusion behavior of water molecules in biological tissue. According to our results, both D_{app} and K_{app} could effectively distinguish between benign and malignant SPLs, which is similar to some recent studies. The results of Das [27] and others show that DKI can distinguish between benign and malignant solitary pulmonary nodules, but DKI did not show a significant advantage compared to conventional DWI. However, it is worth noting that in Das's study, they only used three b-values (0, 500 and 1000 s/mm^2), which may have biased the fitting of DKI, as it is generally believed that water molecule diffusion deviates from a Gaussian distribution only when the maximum b-value is greater than 1000 s/mm^2.

It is generally believed that α can reflect the heterogeneity of microstructure, while K_{app} can represent the complexity of microstructure. Although the exact meaning of α and K_{app} in vivo is not fully understood, our current research results suggest that the negative correlation between them suggests that α and K_{app} may be similar in distinguishing the pathological features of SPLs. However, compared with the conventional ADC obtained from the standard DWI protocol, we did not observe a significant improvement in diagnostic accuracy with α and K_{app}, which may be related to the selection of our ROI. In this study, the ROI was relatively small, only selecting the solid component of the lesion, and the mean value was used to measure each parameter, which may not be conducive to heterogeneity evaluation. Using a whole-volume ROI histogram analysis to evaluate tumor heterogeneity and tumor type may yield better results. In addition, DeLong analysis showed no statistical differences between ADC, DDC, and D_{app} in distinguishing SPLs properties. For the current study, ADC had a high diagnostic accuracy (AUC=0.904), and the DWI extension model did not show a significant advantage in

distinguishing SPL properties. In practical clinical practice, using a single-index DWI model is sufficient to meet the needs of differential diagnosis.

There were several limitations in this study. Firstly, the patient population is relatively small and subtypes of SPLs were not evaluated. Secondly, in this study, ROIs were selected in the solid part of the tumor rather than the entire SPL, which may have led to some selection biases due to the histological heterogeneity of SPL. In the future, further research is needed to investigate the relationship between different DWI models and histological characteristics.

Conclusion

In summary, our findings indicate that the monoexponential, biexponential, stretched-exponential, and diffusion kurtosis models of DWI are potentially valuable imaging tools for the differentiation between benign and malignant SPLs. In addition, DDC obtained from the stretched-exponential model had the highest diagnostic accuracy among different diffusion parameters. The DWI extension model may add potential clinical value for determining the optimal therapeutic approach and predicting the prognosis of SPL patients.

Abbreviations

DWI	Diffusion weighted imaging
DKI	Diffusion kurtosis imaging
IVIM	Intravoxel incoherent motion
SPL	Solitary pulmonary lesion
ROI	Region of interest
ROC	Receiver operating characteristic
ADC	Apparent diffusion coefficient
f	Perfusion fraction
f	Perfusion fraction
ADC_{fast}	Pseudo ADC
ADC_{slow}	True ADC
α	Heterogeneity index
DDC	Distributed diffusion coefficient
AUC	AUC area under the ROC curve

Acknowledgements
We would like to thank all the patients who joined the present study.

Author contributions
All authors contributed to the study's conception and design. KW contributed to the conception of the study, performed the experiment design, and contributed significantly to the analysis and manuscript preparation; GYW helped perform the statistical analysis with constructive suggestions and participated in image acquisition. All authors read and approved the final manuscript.

Funding
This study was funded by Key Laboratory Open Project of Hubei Provincial (2021KFY001), Young Teachers' Independent Research Funding of Wuhan University (2042020kf0127). The funding bodies played no role in the design of the study and collection, analysis, and interpretation of data and in writing the manuscript.

Data availability
The datasets used or analyzed during the current study are available from the corresponding author on reasonable request.

Code or software availability
None.

Declarations

Ethical approval and consent to participate
All procedures performed in studies involving human participants were in accordance with the ethical standards of the Institutional Research Committee at Renmin hospital of Wuhan University and with the 1964 Helsinki declaration and its later amendments or comparable ethical standards.

Informed consent
Informed consent was obtained from all participants.

Consent for publication
Not applicable.

Competing interests
The authors declare no competing interests.

Author details
[1]PET/CT-MRI and Molecular Imaging Center, Renmin Hospital of Wuhan University, Wuhan, Hubei, China
[2]Department of Radiology, Zhongnan Hospital of Wuhan University, Wuhan, Hubei, China

Received: 8 November 2023 / Accepted: 16 December 2024
Published online: 20 December 2024

References

1. Siegel RL, Miller KD, Wagle NS, Jemal A. Cancer statistics, 2023. Ca-Cancer J Clin. 2023;73(1):17–48.
2. Jeong YJ, Lee KS, Jeong SY, Chung MJ, Shim SS, Kim H, et al. Solitary pulmonary nodule: characterization with combined wash-in and washout features at dynamic multi-detector row CT. Radiology. 2005;237(2):675–83.
3. Fu BJ, Lv FJ, Li WJ, Lin RY, Zheng YN, Chu ZG. Significance of intra-nodular vessel sign in differentiating benign and malignant pulmonary ground-glass nodules. Insights Imaging. 2021;12(1):65.
4. Maiga AW, Deppen SA, Mercaldo SF, Blume JD, Montgomery C, Vaszar LT, et al. Assessment of Fluorodeoxyglucose F18-Labeled Positron Emission Tomography for diagnosis of high-risk lung nodules. Jama Surg. 2018;153(4):329–34.
5. Iwano S, Ito S, Tsuchiya K, Kato K, Naganawa S. What causes false-negative PET findings for solid-type lung cancer? Lung Cancer. 2013;79(2):132–6.
6. Cheran SK, Nielsen ND, Patz EJ. False-negative findings for primary lung tumors on FDG Positron emission tomography: staging and prognostic implications. Am J Roentgenol. 2004;182(5):1129–32.
7. Lococo F, Galeone C, Formisano D, Bellafiore S, Filice A, Annunziata T, et al. ^{18}F-fluorodeoxyglucose positron emission tomographic scan in solid-type p-stage-I pulmonary adenocarcinomas: what can produce false-negative results? Eur J Cardio-Thoarc. 2017;51(4):667–73.
8. Chang JM, Lee HJ, Goo JM, Lee HY, Lee JJ, Chung JK, et al. False positive and false negative FDG-PET scans in various thoracic diseases. Korean J Radiol. 2006;7(1):57–69.
9. Koyama H, Ohno Y, Seki S, Nishio M, Yoshikawa T, Matsumoto S, et al. Value of diffusion-weighted MR imaging using various parameters for assessment and characterization of solitary pulmonary nodules. Eur J Radiol. 2015;84(3):509–15.
10. Schwarcz A, Bogner P, Meric P, Correze JL, Berente Z, Pal J, et al. The existence of biexponential signal decay in magnetic resonance diffusion-weighted imaging appears to be independent of compartmentalization. Magn Reson Med. 2004;51(2):278–85.
11. De Santis S, Gabrielli A, Palombo M, Maraviglia B, Capuani S. Non-gaussian diffusion imaging: a brief practical review. Magn Reson Imag. 2011;29(10):1410–6.
12. Le Bihan D, Breton E, Lallemand D, Aubin ML, Vignaud J, Laval-Jeantet M. Separation of diffusion and perfusion in intravoxel incoherent motion MR imaging. Radiology. 1988;168(2):497–505.

13. Bennett KM, Schmainda KM, Bennett RT, Rowe DB, Lu H, Hyde JS. Characterization of continuously distributed cortical water diffusion rates with a stretched-exponential model. Magn Reson Imag. 2003;50(4):727–34.
14. Jensen JH, Helpern JA, Ramani A, Lu H, Kaczynski K. Diffusional kurtosis imaging: the quantification of non-gaussian water diffusion by means of magnetic resonance imaging. Magn Reson Imaging. 2005;53(6):1432–40.
15. Chatziantoniou C, Schoot RA, van Ewijk R, van Rijn RR, Ter Horst S, Merks J, et al. Methodological considerations on segmenting Rhabdomyosarcoma with diffusion-weighted imaging-what can we do better? Insights Imaging. 2023;14(1):19.
16. Van der Hoogt KJJ, Schipper RJ, Winter-Warnars GA, ter Beek LC, Loo CE, Mann RM et al. Factors affecting the value of diffusion-weighted imaging for identifying breast cancer patients with pathological complete response on neoadjuvant systemic therapy: a systematic review. Insights Imaging. 2021;12(1).
17. Hottat NA, Badr DA, Lecomte S, Besse-Hammer T, Jani JC, Cannie MM. Assessment of diffusion-weighted MRI in predicting response to neoadjuvant chemotherapy in breast cancer patients. Sci Rep-UK. 2023;13(1).
18. Yuan M, Zhang Y, Zhu C, Yu T, Shi H, Shi Z, et al. Comparison of Intravoxel Incoherent Motion Diffusion-Weighted MR Imaging with Dynamic contrast-enhanced MRI for differentiating Lung Cancer from Benign Solitary Pulmonary lesions. J Magn Reson Imaging. 2016;43(3):669–79.
19. Liu H, Liu Y, Yu T, Ye N, Wang Q. Evaluation of apparent diffusion coefficient associated with pathological grade of lung carcinoma, before therapy. J Magn Reson Imaging. 2015;42(3):595–601.
20. Zhou SC, Wang YJ, Ai T, Huang L, Zhu TT, Zhu WZ et al. Diagnosis of solitary pulmonary lesions with intravoxel incoherent motion diffusion-weighted MRI and semi-quantitative dynamic contrast-enhanced MRI. Clin Raidol. 2019;74(5).
21. Chen Y, Han Q, Huang Z, Lyu M, Ai Z et al. Value of IVIM in Differential diagnoses between Benign and Malignant Solitary Lung nodules and masses: a Meta-analysis. Front Surg. 2022;9.
22. Le Bihan D, Turner R, Moonen C, Pekar J. Imaging of diffusion and microcirculation with gradient sensitization: design, strategy, and significance. J Magn Reson Imaging. 1991;1(1):7–28.
23. Pekar J, Moonen CT, van Zijl PC. On the precision of diffusion/perfusion imaging by gradient sensitization. Magn Reson Imaging. 1992;23(1):122–9.
24. Thoeny HC, De Keyzer F, Oyen RH, Peeters RR. Diffusion-weighted MR imaging of kidneys in healthy volunteers and patients with parenchymal diseases: initial experience. Radiology. 2005;235(3):911–7.
25. Kwee TC, Galban CJ, Tsien C, Junck L, Sundgren PC, et al. Intravoxel water diffusion heterogeneity imaging of human high-grade gliomas. NMR Biomed. 2010;23(2):179–87.
26. Jin Y, Zhang Y, Cheng J, Zheng D, Hu Y, Monoexponential. Biexponential, and stretched-exponential models using diffusion-weighted imaging: a quantitative differentiation of breast lesions at 3.0T. J Magn Reson Imaging. 2019;50(5):1461–7.
27. Das SK, Yang DJ, Wang JL, Zhang C, Yang HF. Non-gaussian diffusion imaging for malignant and benign pulmonary nodule differentiation: a preliminary study. Acta Radiol. 2017;58(1):19–26.

Publisher's note